ATINER CONFERENCE PAPER SERIES No: IND2013-0818

Athens Institute for Education and Research
ATINER

ATINER's Conference Paper Series
IND2013-0818

Non-Linear Control of Robot aided Belt Grinding Manufacturing Processes

Roland Anderegg
Head of Institute, Professor of Mechatronics
University of Applied Sciences Northwestern
Switzerland
Switzerland

Max Edelmann
Scientific Assistant
University of Applied Sciences Northwestern
Switzerland
Switzerland

ATINER CONFERENCE PAPER SERIES No: IND2013-0818

Athens Institute for Education and Research
8 Valaoritou Street, Kolonaki, 10671 Athens, Greece
Tel: + 30 210 3634210 Fax: + 30 210 3634209
Email: info@atiner.gr URL: www.atiner.gr
URL Conference Papers Series: www.atiner.gr/papers.htm

ISSN **2241-2891**
23/1/2014

An Introduction to ATINER's Conference Paper Series

ATINER started to publish this conference papers series in 2012. It includes only the papers submitted for publication after they were presented at one of the conferences organized by our Institute every year. The papers published in the series have not been refereed and are published as they were submitted by the author. The series serves two purposes. First, we want to disseminate the information as fast as possible. Second, by doing so, the authors can receive comments useful to revise their papers before they are considered for publication in one of ATINER's books, following our standard procedures of a blind review.

Dr. Gregory T. Papanikos
President
Athens Institute for Education and Research

This paper should be cited as follows:

Anderegg, R. and Edelmann, M. (2013) **"Non-Linear Control of Robot aided Belt Grinding Manufacturing Processes"** Athens: ATINER'S Conference Paper Series, No: **IND2013-0818**.

Non-Linear Control of Robot aided Belt Grinding Manufacturing Processes

Roland Anderegg
Head of Institute, Professor of Mechatronics
University of Applied Sciences Northwestern Switzerland
Switzerland

Max Edelmann
Scientific Assistant
University of Applied Sciences Northwestern Switzerland
Switzerland

Abstract

In the production process of faucets, large tolerances, mainly caused by the casting process of the raw part, lead to wide variations in faucet geometry. Additional effort is thus required to manually set the parameters for the robot-guided grinding process. As design products with a complex geometry consisting of several convex and concave surface elements, faucet manufacture poses significant challenges for the robot programmer.

Our contribution towards solving this problem is an analytic description of the manufacturing process to improve the parameters. The developed model of the grinding process consists of a belt grinding machine with contact wheel and the robot which holds the workpiece during the entire manufacturing process. By means of Perturbation Theory, these systems can be divided into a slow and a fast process. The multi-body dynamic system of this model consists of the robot and grinding machine dynamics and additionally of the grinding machine-robot-interaction. This interaction induces a strong nonlinearity, namely the possible loss of contact. Moreover, the behavior of the robot itself is nonlinear, which results in varying compliances depending on the actual position, orientation and trajectory of the robot. For the theoretical analytical model, these influences are respected. In order to validate the derived system model, an experimental setup was designed and analyzed to parameterize, or estimate, significant parameters within the model. As a consequence of the applied research, three representations of the grinding process were obtained and the fundamentals are provided to improve the process by means of control systems.

Keywords: robotics, belt grinding, systems modeling, manufacturing process, industrial automation, non-linear dynamics

Acknowledgements: The authors wish to express their appreciation for the ongoing cooperation with the industrial partner KWC, Unterkulm (Switzerland), in this applied research and development project. They also thank the Swiss Commission for Technology and Innovation CTI for providing a grant towards this project.

Corresponding Author:

Introduction

The main challenge in the production process of design faucets is posed by the complex geometry of their surface. Furthermore, the quality of the finished surface has to be flawless in all transitions between the convex and concave radii which characterize the faucet. Even a minor irregularity on the finished surface means the product must be rejected.

Figure 1. *Black Box Model with difficulties that might arise*

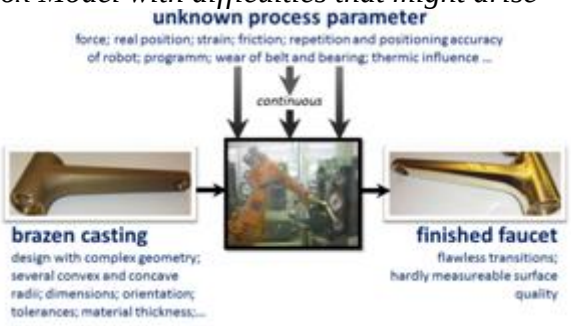

Within the overall production process, the grinding process has the greatest influence on the final appearance of a faucet. Usually the inner part of the brazen casting is made by conventional machining, e.g. by means of turning machines. The grinding process however requires six dimensions of freedom (*DOF*) to machine the complete surface. For this reason, this process step used to be performed manually before the industrial robot manipulator became state of the art. Nowadays the path planning and programming of the robot has to be carried out by skilled workers who must have a competent knowledge of grinding. These workers are responsible for product quality and have to compensate all tolerances in the preproduction processes. Since the process is continuously changing it requires regular fitting, see Figure 1.

Figure 2 illustrates the scope of this work. The grinding process is performed by a robot and a belt grinding machine with a contact wheel. The grinding path and the characteristics of the workpiece are also taken into account.

Figure 2. *Schematic Outline of the Manufacturing Process*

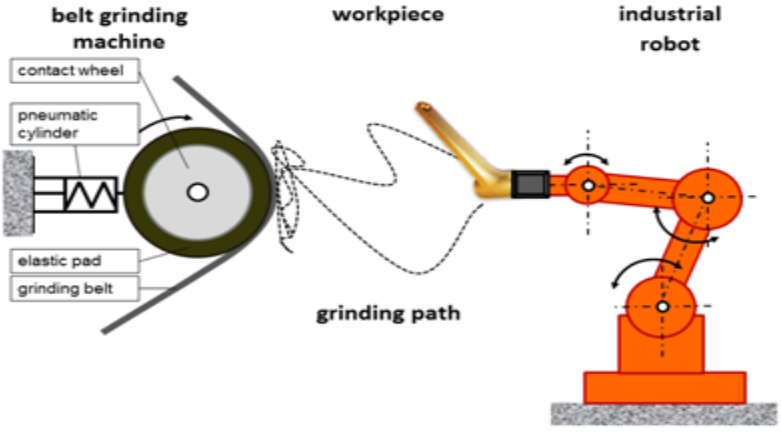

Research Approaches

To overcome the known obstacles inherent in this process, several approaches have been tried, namely various attempts with adaptive training algorithms such as echo state network [1] and an approach to simulate and visualize the belt grinding process [2]. In the field of robotic machining applications an analysis of the system's stiffness was carried out in [3]. Another strategy is to improve the calibration of the robot and the tools in combination with force control [4]. In addition to these procedures the grinding path planning can be optimized using a variety of methods, for instance see [5].

Model of Robot aided Belt Grinding Manufacturing Process

The grinding process requires two mechanical systems: the robot manipulator and the grinding contact wheel, see Figure 3. The analytical model describes the dynamics of each separate system and of the coupled systems. As a third element of the process description, the "robot-contact wheel" interaction force *S(t)* is taken into account. The nonlinear interaction conditions are also presented in this section.

Figure 3. *Analytical Model of the Robot-Grinding Contact Wheel Interaction*

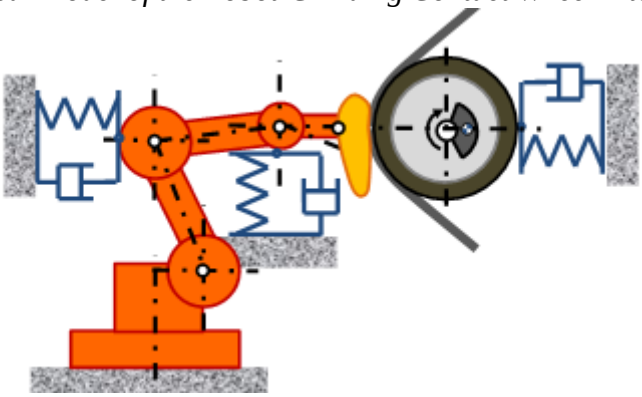

Grinding Process Dynamics

The modeling of the process is based on conventional modeling approaches [6]. Consider the robot as two linked masses that experience a dynamic force at the end-effector. The system therefore consists of two *DOFs* in two dimensions (*x* and *y*). The third dimension in *z*-direction can be neglected for the sake of simplicity in the formulation of the grinding process. The analytical approach to describing this problem is based on a two-link-planar robot model with elastic joints, see Figure 4. The modeled flexibility is considered to be linear and concentrated at the joints, according to [6]. The resulting equations will be derived by the Newton-Euler formulation.

Figure 4. *Model Describing the Robot Dynamics as a Two-Link Planar Robot with Flexible Joints*

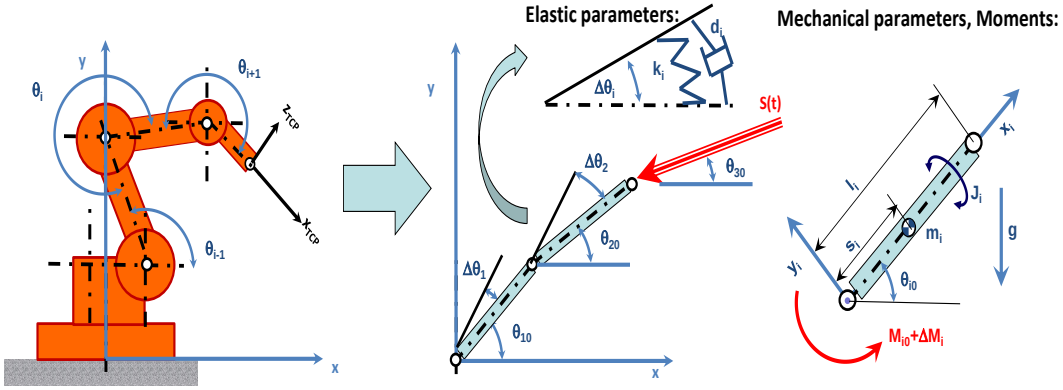

The following parameters are used for the two-link planar robot with flexible joints:

i	[-]	index of the corresponding rigid body
m_i	[kg]	mass of robot arm i
J_i	[kgm^2]	moment of inertia of robot arm i according to local x_i axis
θ_{i0}	[rad]	angle between robot arm i and x axis, is considered to be the robot path planning value
$\Delta\theta_i$	[rad]	infinitesimal difference of robot angle θ_i from the theoretical value θ_{i0}
g	[m/s^2]	=9.81
S	[N]	grinding force, contact force between robot and grinding contact wheel
l_i, s_i	[m]	geometrical parameters of robot arm i
M_i	[Nm]	torque moment acting on robot arm i
M_{i0}	[Nm]	theoretical torque moment for achieving angle θ_{I0}
ΔM_{i0}	[Nm]	infinitesimal torque moment taking into account additional disturbing effects such as robot arm elasticity, grinding force, etc.

Using the principle of virtual energy, the following equations of the robot dynamics result:

$$\left(m_1 s_1^2 + m_2 l_2^2 + J_{z1}\right)\ddot{\theta}_1 - \dot{\theta}_2^2 m_2 s_2 l_1 \sin(\theta_2 - \theta_1) + \ddot{\theta}_2 m_2 s_2 l_1 \cos(\theta_2 - \theta_1) - (m_1 + m_2) g s_1 \cos\theta_1 = M_1 - M_2 + S l_1 \sin(\theta_1 - \theta_3)$$

$$\left(m_2 s_2^2 + J_{z2}\right)\ddot{\theta}_2 + \dot{\theta}_1^2 m_2 s_2 l_1 \sin(\theta_2 - \theta_1) + \ddot{\theta}_1 m_2 s_2 l_1 \cos(\theta_2 - \theta_1) - m_2 g s_2 \cos\theta_2 = M_2 + S l_2 \sin(\theta_2 - \theta_3)$$

Describing the nonlinear vibrations of the angular *DOF* θ_1 and θ_2, the following approach is used:

$$\theta_i \to \theta_{i0} + \Delta\theta_i; \Delta\theta_i << \theta_{i0}$$

Based on Perturbation Theory, the dynamic forces that we observed can be divided into two separate categories:

I. fast, vibrating dynamics of $\Delta\theta_i$
II. slow, smooth dynamics of θ_i, according to the chosen path planning of the robot. The robot actuators are able to generate the driving torques M_1 and M_2 required for holding the planned path.

This can be expressed in Equation 3:

$$\begin{aligned}\left(m_1 s_1^2 + m_2 l_2^2 + J_{z1}\right)\ddot{\theta}_{10} - \dot{\theta}_{20}^2 m_2 s_2 l_1 \sin\left(\theta_{20} - \theta_{10}\right) + \ddot{\theta}_{20} m_2 s_2 l_1 \cos\left(\theta_{20} - \theta_{10}\right) - \left(m_1 + m_2\right) g s_1 \cos\theta_{10} = M_{10} - M_{20} + S_0 l_1 \sin\left(\theta_1 - \theta_3\right)\\ \left(m_2 s_2^2 + J_{z2}\right)\ddot{\theta}_{20} + \dot{\theta}_{10}^2 m_2 s_2 l_1 \sin\left(\theta_{20} - \theta_{10}\right) + \ddot{\theta}_{10} m_2 s_2 l_1 \cos\left(\theta_{20} - \theta_{10}\right) - m_2 g s_2 \cos\theta_{20} = M_{20} + S_0 l_2 \sin\left(\theta_2 - \theta_3\right)\end{aligned}$$

(3)

In addition, the elastic behavior of the robot manipulator is modeled as spring and damping force elements, so that:

$$\Delta M_i := k_i \Delta\theta_i + d_i \Delta\dot{\theta}_i \text{ , e.g. } \Delta M_i := k_i\left(\Delta\theta_i - \Delta\theta_j\right) + d_i\left(\Delta\dot{\theta}_i - \Delta\dot{\theta}_i\right)$$

(4)

Notably, the acting grinding Force S can be regarded as an added disturbance to the system, thus:

$$S \to \Delta S$$

(5)

It can be shown that by applying the addition rules and taking the linearized terms of $\Delta\theta_i$ into account, the following disturbance equations for the vibration dynamics of the robot are obtained:

$$\begin{aligned}&\left(m_1 s_1^2 + m_2 l_2^2 + J_{z1}\right)\Delta\ddot{\theta}_{10} - \dot{\theta}_{20}^2 m_2 s_2 l_1 \left(\Delta\theta_1 - \Delta\theta_2\right)\cos\left(\theta_{20} - \theta_{10}\right) + \Delta\ddot{\theta}_2 m_2 s_1 l_1 \cos\left(\theta_{20} - \theta_{10}\right) + \left(m_1 + m_2\right) g s_1 \Delta\theta_1 \sin\theta_{10} =\\ &\left(m_2 s_2^2 + J_{z2}\right)\Delta\ddot{\theta}_{20} + \dot{\theta}_{10}^2 m_2 s_2 l_1 \left(\Delta\theta_2 - \Delta\theta_1\right)\cos\left(\theta_{20} - \theta_{10}\right) + \Delta\ddot{\theta}_1 m_2 s_2 l_1 \cos\left(\theta_{20} - \theta_{10}\right) + m_2 g s_2 \Delta\theta_1 \sin\theta_{20} =\\ &= \Delta M_1 - \Delta M_2 + \Delta S l_1 \sin\left(\theta_{10} - \theta_{30}\right) + m_2 l_1 s_2 \ddot{\theta}_{20}\left(\Delta\theta_1 - \Delta\theta_2\right)\sin\left(\theta_{10} - \theta_{20}\right) - 2\dot{\theta}_{10}\Delta\dot{\theta}_1 m_2 s_2 l_1 \sin\left(\theta_{20} - \theta_{10}\right) - k_1\Delta\theta_1 + k_2\left(\Delta\theta_2 - \Delta\theta_1\right) - d_1\Delta\dot{\theta}_1 + d_2\left(\Delta\dot{\theta}_2 - \Delta\dot{\theta}_1\right)\\ &= \Delta M_2 + \Delta S l_2 \sin\left(\theta_{20} - \theta_{30}\right) + m_2 l_1 s_2 \ddot{\theta}_{10}\left(\Delta\theta_1 - \Delta\theta_2\right)\sin\left(\theta_{10} - \theta_{20}\right) - 2\dot{\theta}_{20}\Delta\dot{\theta}_2 m_2 s_2 l_1 \sin\left(\theta_{20} - \theta_{10}\right) - k_2\left(\Delta\theta_2 - \Delta\theta_1\right) - d_2\left(\Delta\dot{\theta}_2 - \Delta\dot{\theta}_1\right)\end{aligned}$$

(6)

The averaging formula [7] for the robot dynamics can be given in matrix form:

$$\begin{aligned}&[M]\begin{Bmatrix}\Delta\ddot{\theta}_1\\ \Delta\ddot{\theta}_2\end{Bmatrix} + [D]\begin{Bmatrix}\Delta\dot{\theta}_1\\ \Delta\dot{\theta}_2\end{Bmatrix} + [K]\begin{Bmatrix}\Delta\theta_1\\ \Delta\theta_2\end{Bmatrix} = \underline{\Delta T} + \underline{\Delta S}\\ &[M] = \begin{bmatrix} m_1 s_1^2 + m_2 l_2^2 + J_{z1} & m_2 s_2 l_1 \cos\left(\theta_{20} - \theta_{10}\right)\\ m_2 s_2 l_1 \cos\left(\theta_{20} - \theta_{10}\right) & m_2 s_2^2 + J_{z2}\end{bmatrix}\\ &[D] = \begin{bmatrix} 2\dot{\theta}_{10} m_2 s_2 l_1 \sin\left(\theta_{20} - \theta_{10}\right) + d_1 + d_2 & -d_2\\ -d_2 & 2\dot{\theta}_{20} m_2 s_2 l_1 \sin\left(\theta_{20} - \theta_{10}\right) + d_2\end{bmatrix}\\ &[K] = \begin{bmatrix} -\dot{\theta}_{20}^2 m_2 s_2 l_1 \cos\left(\theta_{20} - \theta_{10}\right) + \left(m_1 + m_2\right) g s_1 \sin\theta_{10} - m_2 l_1 s_2 \ddot{\theta}_{20} \sin\left(\theta_{10} - \theta_{20}\right) + k_1 + k_2 & \dot{\theta}_{20}^2 m_2 s_2 l_1 \cos\left(\theta_{20} - \theta_{10}\right) - m_2 l_1 s_2 \ddot{\theta}_{20} \sin\left(\theta_{10} - \theta_{20}\right) - k_2\\ -\dot{\theta}_{10}^2 m_2 s_2 l_1 \cos\left(\theta_{20} - \theta_{10}\right) - m_2 l_1 s_2 \ddot{\theta}_{10} \sin\left(\theta_{10} - \theta_{20}\right) - k_2 & \dot{\theta}_{10}^2 m_2 s_2 l_1 \cos\left(\theta_{20} - \theta_{10}\right) + m_2 g s_2 \sin\theta_2 + m_2 l_1 s_2 \ddot{\theta}_{10} \sin\left(\theta_{10} - \theta_{20}\right) + k_2\end{bmatrix}\\ &\underline{\Delta T} = \begin{Bmatrix}\Delta M_1 - \Delta M_2\\ \Delta M_2\end{Bmatrix} \qquad \underline{\Delta S} = \begin{Bmatrix}\Delta S l_1 \sin\left(\theta_{10} - \theta_{30}\right)\\ \Delta S l_1 \sin\left(\theta_{20} - \theta_{30}\right)\end{Bmatrix}\end{aligned} \quad (7)$$

Equation (7) shows the mathematical nature of the linearized infinitesimal angles $\Delta\theta_i$ of robot arm *i*. To solve this problem an approach as referred to in Equation (8) might be chosen:

$$\Delta\theta_i = A_i(t)\cos\omega t + B_i(t)\sin\omega t \qquad (8)$$

Due to the nonlinear contact condition between the robot and the contact wheel, A_i and B_i are analytical functions with respect to time *t*, e.g. using the method of the Variation of Constant or the Averaging Method. The excitation frequency *f* is given by the rotating speed of the eccentric grinding contact wheel, while the angular velocity is given by $\omega=2\pi f$. In order to apply the Averaging Method, the assumption of the existence of at least two different time scales has to be made. Regarding the stated problem this means: $\dot{\theta}_{i0} << \Delta\dot{\theta}_i$.

Within the grinding process, an appropriate model for the contact wheel is derived as follows. First, considering the case where the robot is in contact with the grinding contact wheel, the stiffness k_t and damping coefficient d_t are elastic parameters of the contact wheel's elastic covering. The contact wheel itself has an eccentricity *e*, caused particularly by the manufacturing accuracy of the wheel and the unidirectional pressure of the belt. This eccentricity leads to a centrifugal force $m_s e\omega^2$ that excites the whole "robot-contact wheel" system with frequency *f*. Since the actual rotary speed of the wheel is controlled and as a consequence of centrifugal forces acts on the elastic cover, the radius *r* of the wheel may change with respect to frequency *f*, thus *r=r(f)*.

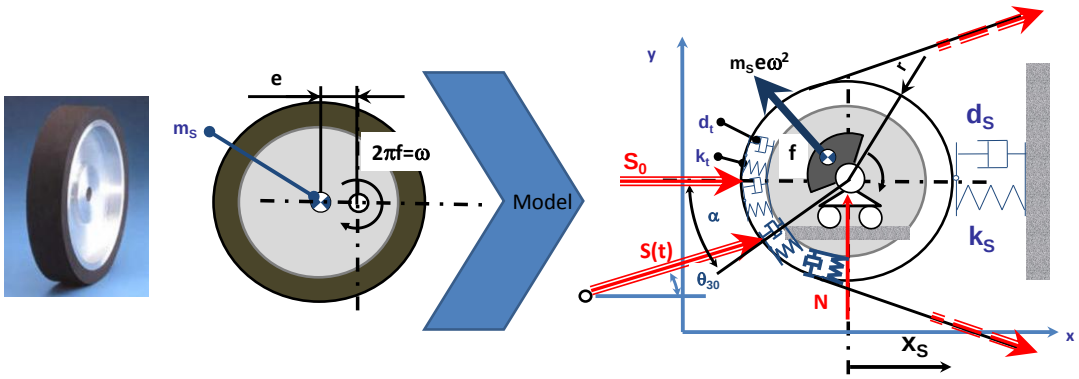

Figure 5: Part of the analytical model describing the contact wheel of the grinding machine

Corresponding to Figure 5 and applying Newton's Law as well as respecting the Law of Impulse and Momentum Conservation, the following equations for the grinding contact wheel are derived:

$$\begin{aligned} m_s\ddot{x}_s + d_s\dot{x}_s + k_s x_s &= S\cos\theta_{30} + m_s e\omega^2\sin\omega t + S_0 \\ m_s\ddot{y}_s &= S\sin\theta_{30} - N + m_s g + m_s e\omega^2\cos\omega t \\ J_s\dot{\omega} &= -S\sin(\theta_{30}-\alpha)r + M \end{aligned} \qquad (9)$$

According to Fig. 5, the following geometrical and mechanical parameters are used to characterize the grinding contact wheel:

m_s	[kg]	mass of contact wheel
J_s	[kgm^2]	moment of inertia of contact wheel
ω	[rad/s]	angular speed of the contact wheel
f	[Hz]	$=\omega/2\pi$frequency of contact wheel
N	[N]	vertical reaction force
r	[m]	$=r(f)$ radius of contact wheel
e	[m]	eccentricity
x_s	[m]	horizontal deflection of grinding contact wheel
k_t	[N/m]	stiffness of elastic covering
k_s	[N/m]	stiffness of wheel suspension
d_t	[Ns/m]	damping of the elastic covering of contact wheel
d_s	[Ns/m]	damping of contact wheel suspension
M	[Nm]	torque moment of contact wheel drive
S_0	[N]	force due to the prestressed belt

The robot manipulator's end-effector and the contact wheel of the grinding machine usually interact during the actual grinding process. This interaction can be characterized by the grinding force $S(t)$ and includes the normal contact force as well as the tangential force (grinding force), hence:

normal contact force: $S(t)\cdot\cos(\theta_{30}-\alpha)$
tangential (grinding) force: $S(t)\cdot\sin(\theta_{30}-\alpha)$ (10)

The relation of both forces is based on Coulomb's Law of Friction, whereas the regime of sliding dry friction is applicable for the grinding process. In brief this is expressed in:

$$F_R=\mu\cdot N_t \Rightarrow \mu=S(t)\cdot\sin(\theta_{30}-\alpha)/S(t)\cdot\cos(\theta_{30}-\alpha)=\tan(\theta_{30}-\alpha) \quad (11)$$

The grinding removal is controlled by the acting contact force $S(t)$, the contact angle θ_{30} and α, and also by the friction coefficient μ. Notably, the coefficient of friction μ is a function of the grinding belt's condition and should be measured during the grinding process.

As Fig. 6 demonstrates, the geometric relationship of the distance between the global center point of the robot and the axle of the rotating contact wheel is given by:

$$u=l_1\cos\theta_{10}+l_2\cos\theta_{20}+r\cdot\cos\alpha+x_s-\Delta\theta_1 l_1\sin\theta_{10}-\Delta\theta_2 l_2\sin\theta_{20} \quad (12)$$

The nonlinear contact between the robot and the grinding contact wheel is simultaneously force and geometrically driven, see Figure 6. Therefore if the condition $u \geq u_0$ *OR* $S \leq 0$ is true, we experience no contact between robot and wheel, thus the grinding force $S=0$.

The nonlinear interaction between the robot arm and the grinding contact wheel could be analytically described as proven in [8], which yields:

$$S(t)\cdot\cos(\theta_{30}-\alpha)=k_t(u-u_0)+d_t(u-u_0)\ \text{if}\ u-u_0>0$$
$$S(t)\equiv 0\ \text{else} \tag{13}$$

The given formulas for the analytical investigation of the nonlinear "robot-contact wheel" dynamics can be simplified and transformed into a translational model including the same number of *DOF*. This transformation is described in detail in the next chapter, followed by a numerical simulation.

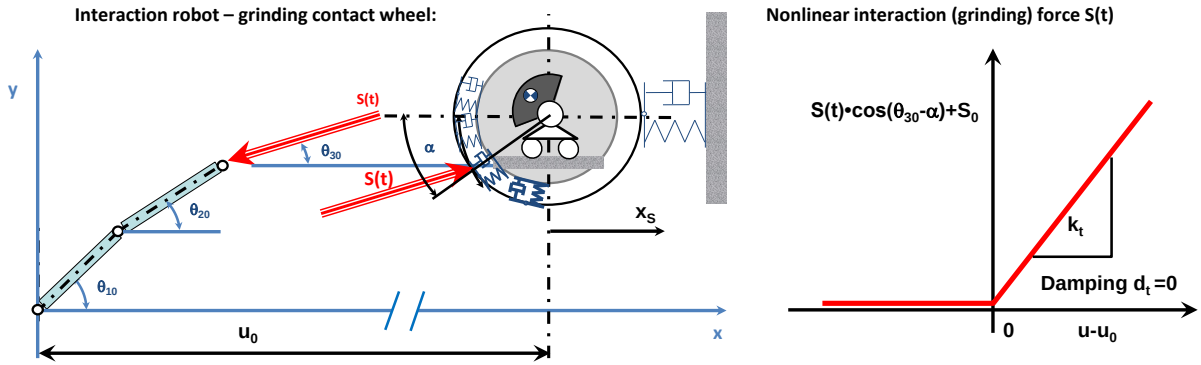

Figure 6: Nonlinear interaction between the robot and the grinding contact wheel, geometrically and contact force driven

The above introduced parameters are defined as:

u	[m]	$u=u(\underline{\theta_{i0}}x_S)$, geometric distance in function of θ_{i0} and x_S
u_0	[m]	undisturbed distance between the global center point of the robot and the origin of the grinding contact wheel
μ	[-]	sliding dry friction coefficient

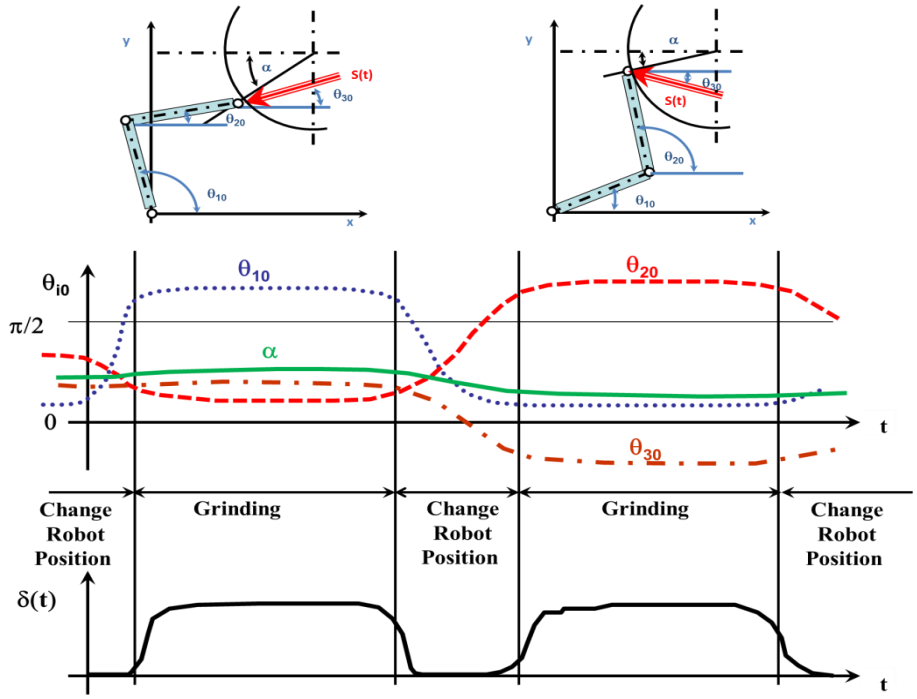

Figure 7: Typical robot parameters during grinding process.
Path planning parameters result in the geometrical intersection *δ(t)*
of robot's tool center point (TCP) and grinding contact wheel surface.

Lumped Parameter Model for Numerical Simulation

For the Lumped Parameter Model, several simplifications using the approach of Perturbation Theory could be applied. The main goal of these investigations is to derive an applicable description of the grinding process.

During this process, the speed of the robot axles is low compared to the time periods when the robot changes its position to rearrange the workpiece. The contact between the robot and the grinding contact wheel is lost for fast maneuvers. The removal of material could be neglected at this stage of modeling, as the influence on the intersection $\delta(t)$ is very small. Figure 7 shows an example of the main characteristics of the robot maneuvers and the resulting robot parameters θ_{i0} and α.

Corresponding to Figure 7, the following assumptions in accordance to the Perturbation Theory are made:

- The geometrical intersection "robot-contact wheel" $\delta(t) := u - u_0$ is the command variable of the simplified simulation model.
- Assuming:
  Therefore: $\dot{\theta}_{i0} \lll \Delta\dot{\theta}_i \qquad \ddot{\theta}_{i0} \lll \Delta\ddot{\theta}_i$

- The difference of the angles is $|\theta_{10}-\theta_{20}|\approx\pi/2$. This assumption does not limit the applications of the simulation results in general.

Using Equation 13 for the grinding force while taking into account the command variable $\delta(t)$ leads to a more elegant expression for the general differential equation, see Equation (7):

$$[M]\begin{Bmatrix}\Delta\ddot{\theta}_1\\ \Delta\ddot{\theta}_2\end{Bmatrix}+[D]\begin{Bmatrix}\Delta\dot{\theta}_1\\ \Delta\dot{\theta}_2\end{Bmatrix}+[K]\begin{Bmatrix}\Delta\theta_1\\ \Delta\theta_2\end{Bmatrix}=\underline{\Delta T}+\underline{\Delta S} \tag{14}$$

wherein the moment vector is set equal to gravitational forces:

$$\underline{\Delta T}\equiv\begin{Bmatrix}\Delta M_1-\Delta M_2\\ \Delta M_2\end{Bmatrix}=\begin{Bmatrix}(m_1+m_2)gs_1\sin\theta_{10}\\ m_2gs_2\sin\theta_{20}\end{Bmatrix} \tag{15}$$

Consequently, these assumptions lead to the following simplified matrix forms:

$$[M]=\begin{bmatrix}m_1s_1^2+m_2l_2^2+J_{z1} & m_2s_2l_1\cos\overbrace{(\theta_{20}-\theta_{10})}^{\pi/2}\\ m_2s_2l_1\underbrace{\cos(\theta_{20}-\theta_{10})}_{\pi/2} & m_2s_2^2+J_{z2}\end{bmatrix}=\begin{bmatrix}m_1s_1^2+m_2l_2^2+J_{z1} & 0\\ 0 & m_2s_2^2+J_{z2}\end{bmatrix} \tag{16}$$

$$[D]=\begin{bmatrix}2\overset{\approx 0}{\dot{\theta}_{10}}m_2s_2l_1\sin(\theta_{20}-\theta_{10})+d_1+d_2 & -d_2\\ -d_2 & 2\overset{\approx 0}{\dot{\theta}_{20}}m_2s_2l_1\sin(\theta_{20}-\theta_{10})+d_2\end{bmatrix}=\begin{bmatrix}d_1+d_2 & -d_2\\ -d_2 & d_2\end{bmatrix} \tag{17}$$

$$[K]=\begin{bmatrix}-\dot{\theta}_{20}^2m_2s_2l_1\cos(\theta_{20}-\theta_{10})+(m_1+m_2)gs_1\sin\theta_{10}-m_2l_1s_2\ddot{\theta}_{20}\sin(\theta_{10}-\theta_{20})+k_1+k_2 & \dot{\theta}_{20}^2m_2s_2l_1\cos(\theta_{20}-\theta_{10})-m_2l_1s_2\ddot{\theta}_{20}\sin(\theta_{10}-\theta_{20})-k_2\\ -\dot{\theta}_{10}^2m_2s_2l_1\cos(\theta_{20}-\theta_{10})-m_2l_1s_2\ddot{\theta}_{10}\sin(\theta_{10}-\theta_{20})-k_2 & \dot{\theta}_{10}^2m_2s_2l_1\cos(\theta_{20}-\theta_{10})+m_2gs_2\sin\theta_{20}+m_2l_1s_2\ddot{\theta}_{10}\sin(\theta_{10}-\theta_{20})+k_2\end{bmatrix} \tag{18}$$

Moreover, by respecting the dynamics and the choice of $\underline{\Delta T}$ we derive:

$$[K]=\begin{bmatrix}k_1+k_2 & -k_2\\ -k_2 & k_2\end{bmatrix} \tag{19}$$

As a third equation, the differential equation of the grinding contact wheel is attached (9) and induces a three-*DOF* system:

$$[M]\begin{Bmatrix}\Delta\ddot{\theta}_1\\ \Delta\ddot{\theta}_2\end{Bmatrix}+[D]\begin{Bmatrix}\Delta\dot{\theta}_1\\ \Delta\dot{\theta}_2\end{Bmatrix}+[K]\begin{Bmatrix}\Delta\theta_1\\ \Delta\theta_2\end{Bmatrix}=\begin{Bmatrix}Sl_1\sin(\theta_{10}-\theta_{30})\\ Sl_1\sin(\theta_{20}-\theta_{30})\end{Bmatrix}=\begin{Bmatrix}S_1\\ S_2\end{Bmatrix}$$
$$m_s\ddot{x}_s+d_s\dot{x}_s+k_sx_s=S\cos\theta_{30}+m_se\omega^2\sin\omega t+S_0=S_3+m_se\omega^2\sin\omega t+S_0 \tag{20}$$

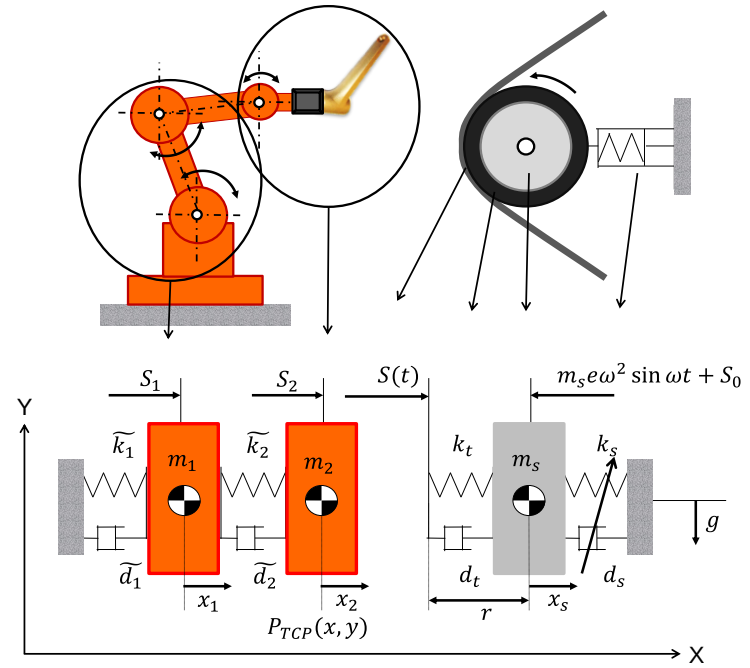

Figure 8: Lumped Parameter Model for numerical simulation. All DOFs are translational according to Equation (22)

Referring to Figure 8, the Lumped Parameter Model for numerical simulations might be defined as follows. The system of differential equations describes the grinding process only in cases of contact between the robot and the grinding machine and is summarized in the formula below:

(21) $$[M]\underline{\ddot{x}} + [D]\underline{\dot{x}} + [K]\underline{x} = \underline{S}$$

whereby the rotational *DOF*s might be transformed into translational *DOF*s using a simple arithmetic formula:

- $x_i := \Delta\theta_i \; a$, wherein the parameter a, the characteristic length in [m], might be arbitrarily chosen.
- Therefore, the mechanical parameters of the robot are transformed.

Likewise:

$$\tilde{m}_i := m_i / a \qquad \tilde{d}_i := d_i / a \qquad \tilde{k}_i := k_i / a$$

- The nonlinear forces S_i are not touched.

In conclusion, we obtain the following matrix differential equation:

$$\begin{bmatrix} \tilde{m}_1 & 0 & 0 \\ 0 & \tilde{m}_2 & 0 \\ 0 & 0 & m_s \end{bmatrix} \begin{Bmatrix} \ddot{x}_1 \\ \ddot{x}_2 \\ \ddot{x}_s \end{Bmatrix} + \begin{bmatrix} \tilde{d}_1 + \tilde{d}_2 & -\tilde{d}_2 & 0 \\ -\tilde{d}_2 & \tilde{d}_2 & 0 \\ 0 & 0 & d_s \end{bmatrix} \begin{Bmatrix} \dot{x}_1 \\ \dot{x}_2 \\ \dot{x}_s \end{Bmatrix} + \begin{bmatrix} \tilde{k}_1 + \tilde{k}_2 & -\tilde{k}_2 & 0 \\ -\tilde{k}_2 & \tilde{k}_2 & 0 \\ 0 & 0 & k_s \end{bmatrix} \begin{Bmatrix} x_1 \\ x_2 \\ x_s \end{Bmatrix} = \begin{Bmatrix} S_1 \\ S_2 \\ S_0 \cos\theta_{30} + m_s e\omega^2 \sin \omega t + S_0 \end{Bmatrix}$$

(22)

For definition of S_i, see Equation (20).

The parameters of the linearized systems of Equation (22) for numerical simulation are:

- For the robot subsystem:

x_i	[m]	translational degree of freedom (*DOF*)
$\tilde{k}_i$	[N/m]	translational stiffness of the robot, which depends on the current position
$\tilde{d}_i$	[Ns/m]	translational damping, which may depend on the current position
m_i	[kg]	mass of link *i* $\tilde{m}_1 = m_1 s_1^2 + m_2 l_2^2 + J_{z1}$ $\tilde{m}_2 = m_2 s_2^2 + J_{z2}$

- For the grinding machine subsystem:

x_s	[m]	translational degree of freedom (*DOF*)
$k_{t,}$ k_s	[N/m]	translational stiffness of the elastic pad and the pneumatic cylinder
$d_{t,}$ d_s	[Ns/m]	translational damping of the elastic pad and the pneumatic cylinder
m_s	[kg]	mass of contact wheel
S_0	[N]	force due to the prestressed belt
S_i	[N]	force due to excitation, e.g. of the contact wheel (i=1, 2)
$S(t)$	[N]	nonlinear contact force

Numerical Simulation and Validation

In order to analyze the dynamic behavior of the derived system, a numerical simulation model was developed according to Equation (22) with an implementation of the nonlinear contact condition according to Equation 13. By aid of several practical measurements on the real system, unknown parameters of the process model were evaluated. Further internal process factors had been estimated to complete the model.

Regarding the measurement results, the yield model might be extended by excitation sources. Considering Equation (9), the acting force on the "grinding contact wheel" system is characterized by the rotation of the contact wheel itself, but in fact other effects of the grinding machine also come into play. They will be summarized as residuals, e.g. the driven wheel, all assistance wheels, vibrations of the belt, the transmission of the belted gear, etc. Thus, the right-hand side of Equation (9) becomes an enhanced equation and can be written as:

$$S\cos\theta_{30} + m_s e\omega^2 \sin\omega t + S_0 \Rightarrow S\cos\theta_{30} + m_s e\omega^2 \sin\omega t + S_0 + \sum_i \lambda_i \cos\omega_i t \quad (24)$$

Within the executed simulations, only the dominating amplitudes and frequencies are respected, see Figure 11 (r.).

ω_i	[rad/s]	frequency of the i^{th} additional element exciting the system
λ_i	[N]	force amplitude of the i^{th} additional element exciting the system

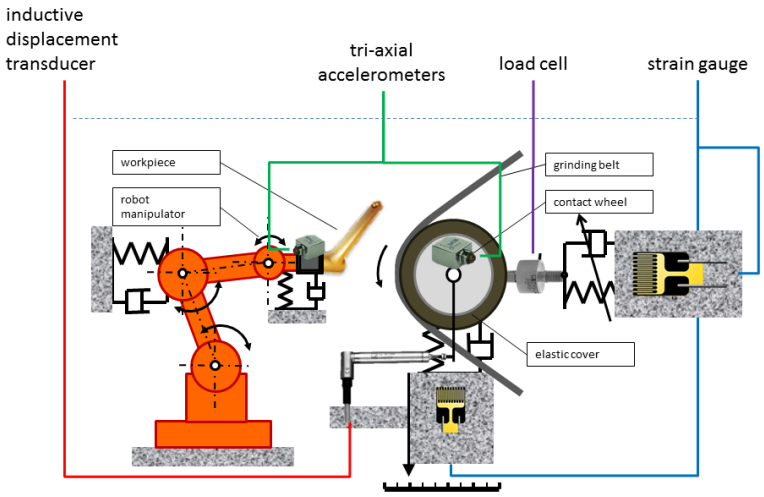

Figure 9: Measurement setup

In order to validate the system description, several sensors are mounted. Tri-axial accelerometers are applied. Additionally, an inductive displacement transducer, a load cell for tensile and compressive forces and strain gauges are directly installed on the grinding machine, see Figure 9. The grinding process is consequently fully observable.

For test measurements, a short, defined grinding period is recorded and step by step the process parameters are varied. However, characteristic phenomena of the process can be verified with this approach, for instance, the increasing radius of the contact wheel, see Figure 10 (left), or the position dependent compliance of the tested robot. Moreover, the assumptions made to model this process according to the Perturbation Theory can be proved, see Figure 10 (right.). Where it is shown that the grinding process has a fast periodic influence on the robot (right side, left column) and on the other hand, if the robot is not in contact, only the motion profile is relevant (right side, right column).

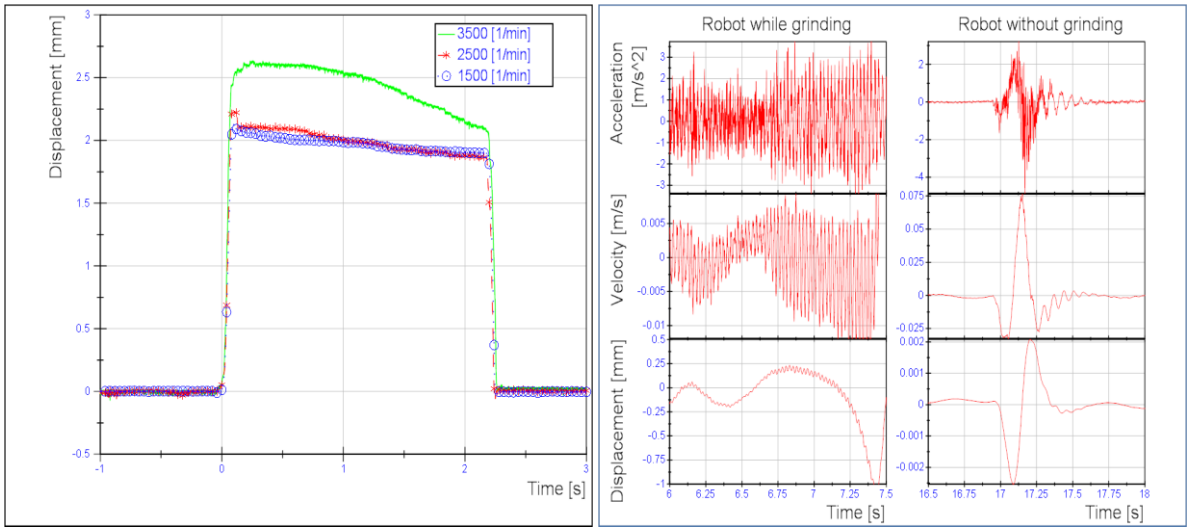

Figure 10: Displacement measurement x_s compared for different frequencies f while moving along the same path (left).
Measurements of the robot comparing the behavior of the robot's TCP while in contact with the grinding belt (right).

As a matter of fact, the tested system is an adequate dynamic system and therefore frequencies are relevant. The results of the numerical simulation can be represented in the time and frequency domains and throughout compared with the data from the measurements, see Figure 11 and 12.

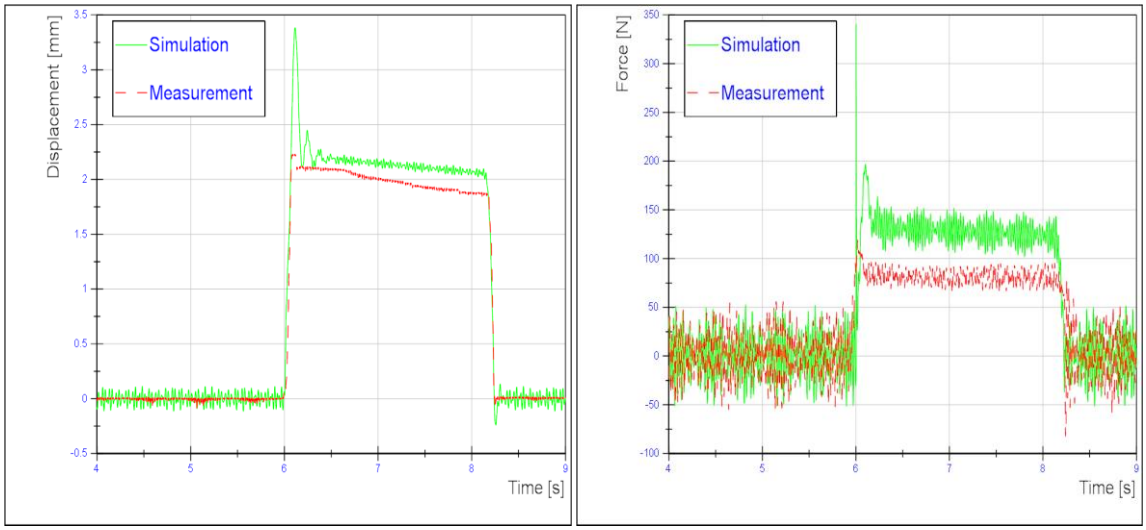

Figure 11: Displacement of the contact wheel (left). Acting force, measured at grinding machine (right)

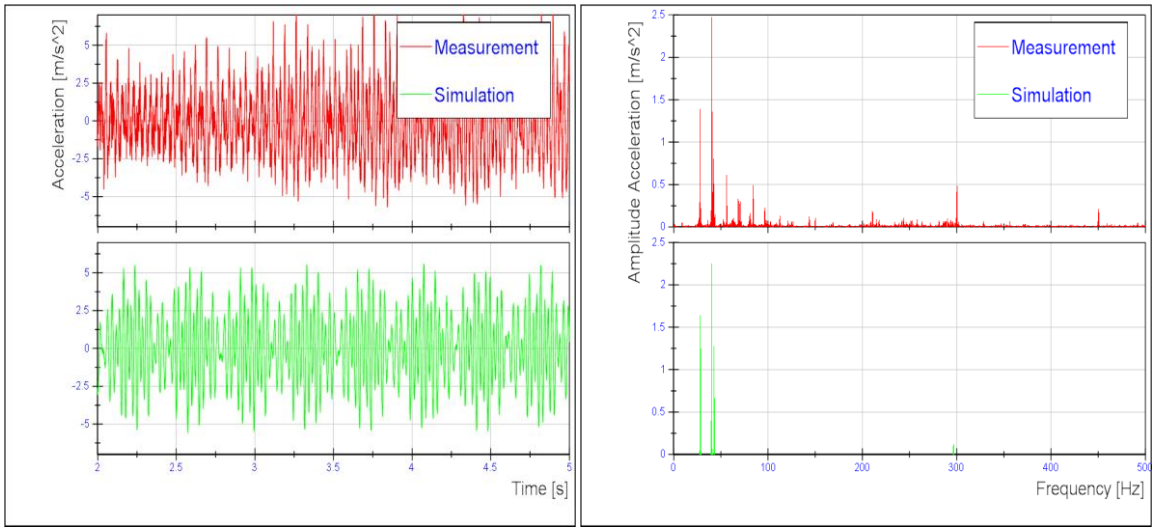

Figure 12: Comparing measurement with simulation in time and frequency domains.

Overall, comparing the practical measurements with output of the numerical simulation model and the theoretical description a sufficient correlation is found. The remaining differences are caused by simplifying the robot's *DOFs*, idealized system factors such as no disturbing vibrations, measurement inaccuracies and errors in the parameter evaluation.

Conclusion

Three representations for the grinding process are obtained, first a mathematical description, second a numerical simulation model and third expressive data based on practical measurements. As a result, a detailed description of the grinding process is achieved. Indeed, the practical measurements within a real system indicate that this description is valid. A notable aspect of this work is its theoretical approach based on Perturbation Theory, while respecting the flexibility in the joints, which has a crucial influence on the whole system dynamics.

In practice, several factors are unknown, since the industrial robot manipulator is usually a proprietary product with manufacturer-specific properties. Hence, as the desired value for removal is considered to be small in contrast to the correspondingly large workspace of the robot, it is difficult to guarantee the required accuracy for this dynamic process. Nevertheless, based on our work and applying approaches from control systems theory, the grinding process can be improved. Considering the whole issue, the grinding process is purely a force-driven process, whereas a robot is a path-driven manipulator. To merge these two contrary systems, it is common practice to use passive elements. Hence, solutions consisting of passive elements constantly meet with inaccuracies. This work provides fundamentals to develop an active, robot aided belt grinding system that guarantees the required forces by means of control systems.

References

Hongbo Lv, Yixu Song, Peifa Jia. "An Adaptive Modeling Approach Based on ESN for Robotic Belt Grinding". Proceedings of the 2010 IEEE, International Conference on Information and Automation. Harbin, China. pp. 787-792, 2010.

Xiangyang Ren, Bernd Kuhlenkötter. "Real-time simulation and visualization of robotic belt grinding processes".International Journal of Advanced Manufacturing Technology. Springer Science+Business Media B.V.. London, pp. 1090-1099, 2008.

E. Abele, M. Weigold, S. Rothenbücher. "Modeling and Identification of an Industrial Robot for Machining Applications". CIRP Annals - Manufacturing Technology, Volume 56, Issue 1. ElSevier B.V.. pp. 387–390, 2007.

Yunquan Sun, David J. Giblin, Kazem Kazerounian. "Accurate robotic belt grinding of workpieces with complex geometries using relative calibration techniques". Robotics and Computer-Integrated Manufacturing, Volume 25, Issue 1. Elsevier B.V.. pp. 204-210, 2009.

Wei WANG, Chao YUN. "A Path Planning Method for Robotic Belt Surface Grinding". Chinese Journal of Aeronautics, Volume 24, Issue 4. Elsevier B.V.. pp. 520–526, 2011.

B. Siciliano, O. Khatib. "Springer Handbook of Robotics". Springer Science+Business Media B.V.. 2008

Sanders, Jan A., Verhulst, Ferdinand, Murdock, James. "Averaging Methods in Nonlinear Dynamical Systems". 2nd ed. Springer Science+Business Media B.V.. 2007

R. Anderegg and L. Recher, “Control of chaotic vibrations using the principle of autoparametric resonances,” Mechatronics 2010, ETH Zurich, Switzerland, June 2010.